Cu and Zn ordering in aurichalcite

J. M. CHARNOCK[1], P. F. SCHOFIELD[2], C. M. B. HENDERSON[1], G. CRESSEY[2] AND B. A. CRESSEY[3]

[1]Department of Earth Sciences, University of Manchester, Oxford Road, Manchester, M13 9PL, UK
[2]Department of Mineralogy, Natural History Museum, Cromwell Road, London, SW7 5BD, UK
[3]Department of Geology, University of Southampton, Southampton Oceanography Centre, Southampton, SO14 3ZH, UK

Abstract

The advantages of X-ray absorption spectroscopy have been utilized to assess the Cu and Zn ordering in aurichalcite, $(Cu_{5-x}Zn_x)(OH)_6(CO_3)_2$. We have examined one hydrozincite sample and three aurichalcite samples in which the Cu:Zn ratios are in the range 1:3 to 2:3. Copper 2p XAS confirms that there is no monovalent copper in aurichalcite and that in each sample the copper might be distributed across more than one metal site. EXAFS, at the Cu and Zn K-edges, shows that the copper atoms preferentially enter the Jahn-Teller elongated, octahedral ($M2$) and trigonal bipyramidal ($M4$) sites, with the zinc atoms entering the more regular octahedral ($M1$) and tetrahedral ($M3$) site. Substantial solid solution towards the zinc rich region is facilitated by the substitution of copper by zinc on the $M2$ and $M4$ sites. This information, not easily obtained by X-ray diffraction, substantially enhances the understanding of the structure of aurichalcite.

KEYWORDS: aurichalcite, hydrozincite, Cu and Zn ordering, EXAFS.

Introduction

AURICHALCITE, $(Cu_{5-x}Zn_x)(OH)_6(CO_3)_2$, is a relatively rare secondary mineral found in copper ore bodies. It appears as aggregates or tufts of light blue/green needles and blades. Braithwaite and Ryback (1963) reported two modes of formation of aurichalcite, either as pseudomorphs after malachite or azurite induced by the reaction with Zn-bearing solutions as at Tsumeb, Namibia, or as a primary precipitate from the low-temperature reaction of Zn-bearing solutions with copper sulphide minerals as at Masson Hill, U.K.

Industrially, synthetic aurichalcite has an important use as a catalyst precursor for hydrogenation processes and, as such, has recently been the focus of a number of studies (Sengupta et al., 1995; Herman et al., 1993; Pollard et al., 1992; Porta et al., 1991). Despite this important application, the structure of aurichalcite was only recently solved by Harding et al. (1994). The small crystallite size and twinned nature of aurichalcite posed serious problems for attempts at structural solution, resulting in an incorrect choice for the unit cell by earlier workers (Jambor and Pouliot, 1965). Indeed, Harding et al. (1994) required the application of synchrotron

radiation to solve the structure from a twinned microcrystal only 5 μm thick. Although Harding et al. (1994) stated that knowledge of the Cu/Zn distribution was important, they were limited to postulating that the tetrahedral sites are probably occupied by zinc and the other sites by zinc and copper. Considering the problems discussed by Harding et al. (1994) more conclusive information concerning the metal distribution will be difficult to obtain by X-ray diffraction as the scattering factors for Cu and Zn are so similar.

The lack of reliable structural information has meant that, hitherto, the interpretation of EXAFS data on aurichalcite could only be based on comparisons with the hydrozincite structure. There are, however, significant differences in these two structures and as a consequence previous EXAFS analyses may be erroneous. For example, Couves et al. (1991) used combined X-ray absorption and diffraction to assess the occupancy of Zn and Cu over two octahedral sites and one tetrahedral site. As will be seen in the next section, the structure of aurichalcite is more complex than this, and hence this conclusion may be oversimplified. In this paper we discuss the ordering of Cu and Zn in three samples of aurichalcite, with differing Cu:Zn ratios, using
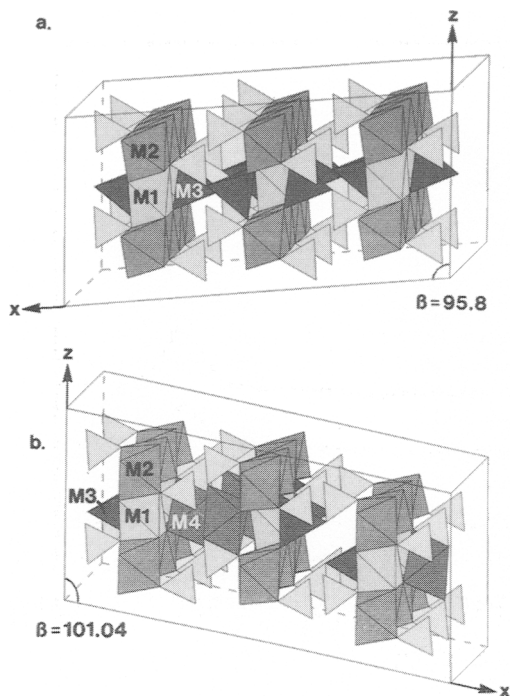
FIG. 1. The crystal structure of (*a*) hydrozincite and (*b*) aurichalcite showing the different metal sites. Both structures are viewed along the *b* axis with the *c* axis vertical.

EXAFS data refined in view of the crystal structure information now available.

The three aurichalcite samples and the hydrozincite sample used in this study are from the mineral collection at the Natural History Museum, London, U.K. The aurichalcites are BM 1937,1355 from Big Cottonwood Canyon, Salt Lake County, Utah; BM 1964,702 from Ojela Mine, Durango, Mexico; and BM 1983,97 (as used by Harding *et al.*, 1994) from Pima County, Arizona. The hydrozincite is number BM 1979,215 from Shāh Kūh, Eṣfahān, Iran.

Crystal structure

The crystal structure of auricalchite was finally solved by Harding *et al.* (1994) and found to be related to that of hydrozincite, $Zn_5(OH)_6(CO_3)_2$ (Ghose, 1964). Both aurichalcite and hydrozincite, shown in Fig. 1, possess double layers of close packed oxygen layers parallel to (100). Within this double layer is the octahedral *M*1 site and the tetragonally elongate *M*2 site. On the opposing sides of this double layer are the tetrahedral *M*3 site and the trigonal bipyramidal *M*4 site. Layers are bound

together on one side by hydrogen bonding, between the hydroxyl groups and an oxygen from a carbonate group, and on the other side there is metal-oxygen bonding. Hydrozincite, on the other hand possesses no trigonal bipyramidal metal sites, having twice as many tetrahedral sites instead and there is metal-oxygen bonding involved between all layers.

Characterization

X-ray diffraction, using a Philips PW2400 scanning diffractometer and Cu-*K*α radiation, showed that all the specimens except BM 1964,702 were single phase. Specimen BM 1964,702 also contains murdochite (Cu_6PbO_8); however, careful mineral picking ensured that there was no obvious mixing of the two phases in the samples studied. Indeed, no murdochite was observed in the mineral separated by XRD, SEM, using a JEOL 6400, and TEM, using a JEOL 2000FX.

Because aurichalcite is so soft (H∼2) and extremely fragile, it is unsuitable for the manufacture of polished surfaces for electron microprobe analysis. Therefore, crystal fragments were mounted directly on adhesive conducting discs and lightly gold coated for imaging and analysis using a JEOL 6400 analytical SEM. The Cu:Zn ratios determined by EDS showed some variation in each sample; this could reflect a true variation between different crystals, or this could be a function of X-ray take-off angle, although in the absence of a flat polished surface care was taken to choose horizontally flat crystals for analysis. The Zn/(Zn + Cu) values obtained are 0.81 (± 0.01) for BM 1937,1355; 0.58 (± 0.04) for BM 1964,702; and 0.62 (± 0.04) for BM 1983,97.

Cu 2p XAS

Experimental methods

The aurichalcite samples were thoroughly ground and mixed with ultra-pure graphite, to a sample:-graphite ratio of 4:1, in an agate pestle and mortar, and smeared onto aluminium plates. The Cu 2p XAS spectra were recorded in total electron yield mode on station 3.4 of the Daresbury Synchrotron Radiation Source, U.K., employing a double crystal mono-chromator equipped with beryl $10\bar{1}0$ crystals (MacDowell *et al.*, 1988). The energy was calibrated to the Cu L_3 peak of CuO at 931.2eV ± 0.05eV and the energy resolution was ∼400meV.

Results

The Cu 2p XAS spectra of the aurichalcite samples are shown in Fig. 2. The three spectra show a single L_3
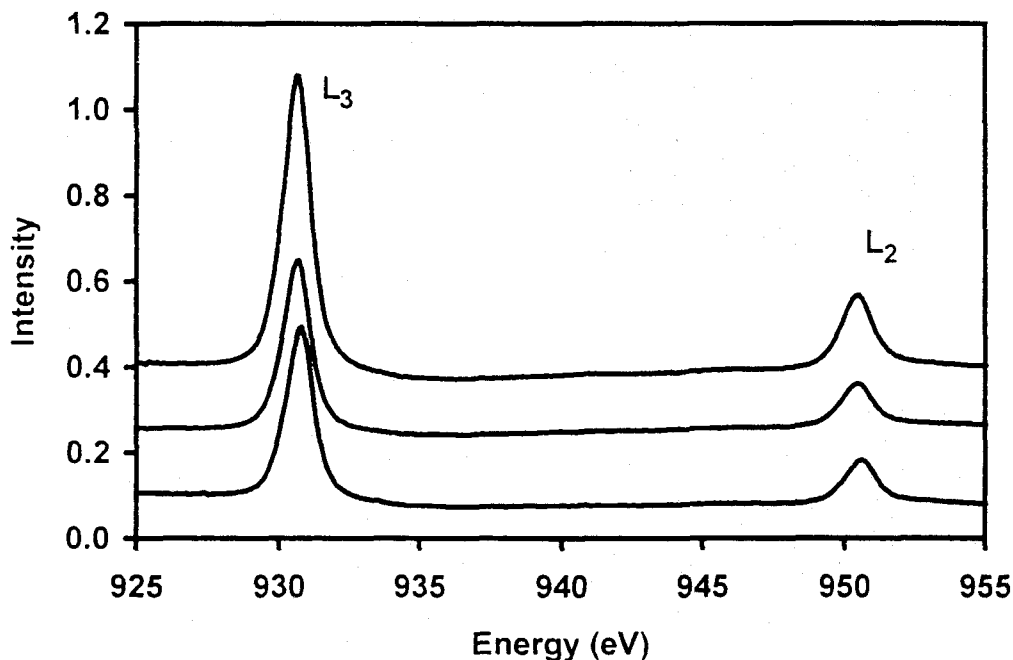
FIG. 2. Cu 2p XAS spectra for aurichalcites BM 1964,702 (top), BM 1983,97 (middle) and BM1937,1355 (bottom).

peak at about 930eV and a single L_2 peak at about 950eV. van der Laan *et al.* (1992) showed that the L_3 peak for divalent copper, in a range of minerals, occurs in the energy range 930.5–931.2eV, whereas that for monovalent copper occurs within the higher energy range of 931.9–933.4eV. Furthermore the L_3 peak for monovalent copper is accompanied by a large increase in intensity just above this leading peak. The L_3 peaks for BM 1964,702, BM 1983,97 and BM 1937,1355 occur at 930.43eV, 930.43eV and 930.64eV ($\pm$ 0.05eV) respectively, and there is no accompanying intensity increase above any of these peaks. This indicates that the copper in these aurichalcite samples is predominantly present as Cu^{2+}.

The L_3 peak for divalent copper represents the electron transition $2p^6 3d^9 \rightarrow 2p^5 3d^{10}$ and as such should be symmetrical, reflecting a single line without multiplet splitting. All the L_3 peaks in Fig. 2, however, appear to be asymmetric. Furthermore, it appears that a shoulder is resolved on the low energy side of the L_3 peak for BM 1937,1355. This asymmetry might be due to the superposition of more than one absorption peak and, as such, would represent Cu^{2+} sites of differing electronic structure. Thus, as may be expected from crystal chemistry, it follows that in all the samples Cu^{2+} is located in more than one site. Such additional features have been used previously to model site occupancies in

$(Zn_x Cu_{1-x})WO_4$ (Schofield *et al.*, 1993), but are not sufficiently detectable for such analysis here. If these features are indeed due to multiple site occupancies, then the different energy and shape of the L_3 peaks for BM 1964,702 and BM 1983,97 from that of BM 1937,1355 may be assigned to an extra absorption component representing the existence of an extra Cu^{2+} site. This distribution of Cu between different sites may also be related to bulk chemistry as BM 1937,1355 with a Zn/(Zn + Cu) ratio higher by about 0.15 than the other two samples, has a more resolved shoulder. These features are very subtle and consequently, from the Cu 2p XAS alone, it is not possible to speculate any further on the cation ordering and occupancies of Cu and Zn in the four distinct sites of aurichalcite. For this we have used another aspect of XAS, namely extended X-ray absorption fine structure (EXAFS) at both the Cu and Zn K-edges.

Cu and Zn K-edge EXAFS

Experimental methods

The hydrozincite and aurichalcite samples were thoroughly ground in an agate pestle and mortar and pressed into thin plastic sample holders using Sellotape windows. The EXAFS spectra were
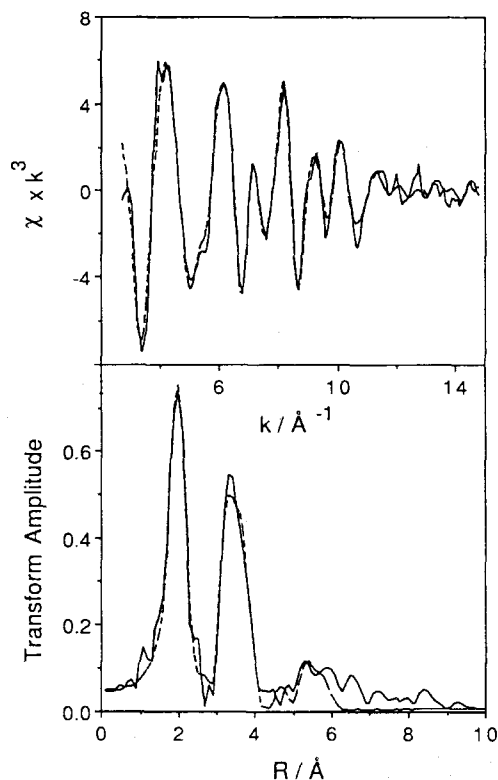
FIG. 3. 80K Zn EXAFS (solid line, top) and Fourier transform (solid line, bottom) and the corresponding bets fit (broken lines) of hydrozincite.

Radiation Source, U.K., operating in multibunch mode at an energy of 2 GeV with an average current of 150 mA. The double crystal Si(111) monochromator was detuned to 50% rejection of the incident beam in order to remove harmonic contamination. For low-temperature measurements (~ 80 K) the samples were attached to aluminium holders on a cryostat cold-finger, cooled in liquid nitrogen, and placed in an evacuable cryostat chamber. The temperature was maintained by conduction from a reservoir of liquid nitrogen.

The monochromator angle was calibrated to either Cu or Zn metal foils, and the raw spectra were background subtracted using the Daresbury program EXBACK. The isolated EXAFS data were analysed using EXCURV92 (Binsted *et al.*, 1991) employing the rapid curved wave theory (Lee and Pendry, 1975: Gurman *et al.*, 1984). Phase shifts were derived from *ab initio* calculations using Hedin-Lundqvist potentials (Hedin and Lundqvist, 1969) and von Bart ground states. For each spectrum a theoretical fit was obtained by adding shells of backscattering atoms around the central absorber atom and iterating the absorber-scatterer distances, R, and the Debye-Waller type factors, $2\sigma^2$. The Debye-Waller factors include contributions from the thermal motion of the absorber-scatterer pairs and also the static contribution from any variation in R between the scatterers in one shell.

The magnitude of the absorption edge height is a function of the content of the absorbing metal atom (Cu or Zn) and of its absorption cross section. Copper and zinc have very similar absorption cross sections, and therefore the ratios of the step heights for Cu and Zn in the same sample can be used as an approximate indicator of the Cu:Zn ratio. The ratios determined in this way are in excellent agreement with the ratios

recorded in transmission mode at the Cu and Zn K-edges, on station 7.1 of the Daresbury Synchrotron

TABLE 1. Comparison of the crystal structure of hydrozincite (Ghose, 1964) with parameters derived from the Zn K-edge EXAFS spectra at ambient temperature and *ca.* 80K. The R-factors for the fit at ambient is 22.2 and for the fit at *ca.* 80K is 23.9

Crystal Structure (weighted average of three zinc sites)			EXAFS (ambient)		EXAFS (ca. 80 K)	
Shell*	R/Å	Range/Å	R/Å	$2\sigma^2/\text{Å}^2$	R/Å	$2\sigma^2/\text{Å}^2$
1.6 × O	1.95	1.856–1.984	1.96	0.010	1.96	0.007
3.6 × O	2.10	2.043–2.159	2.07	0.015	2.06	0.014
0.4 × Zn	2.99	–	3.05	0.012	3.05	0.008
1.6 × Zn	3.18	–	3.18	0.012	3.18	0.011
5.6 × Zn	3.55	3.31–3.60	3.55	0.025	3.55	0.024
0.8 × Zn	4.61	–	4.56	0.020	4.57	0.018
0.8 × Zn	5.08	–	5.20	0.012	5.19	0.008
3.6 × Zn	5.40	5.38–5.42	5.41	0.024	5.42	0.021

* Shells of light atoms (O and C) are omitted beyond the inner coordination sphere

gained from the EDS probe analyses, giving values for Zn/(Zn + Cu) of 0.76 for BM 1937,1355, 0.58 for BM 1964,702 and 0.60 for BM 1983,97.

Data analysis

(i) *Hydrozincite*. In the structure of hydrozincite (Ghose, 1964) the zinc occupies three sites, two octahedral and one tetrahedral, with multiplicities in the ratio 1:2:2. The EXAFS will be an average of the contributions from each site. In order to analyse the data the numbers of scatterers in each shell were fixed at the crystallographic weighted averages, and the absorber-scatterer distances and Debye-Waller type factors allowed to vary until the best fit was found. Oxygen and carbon atoms were not included in the simulations beyond the inner coordination sphere, as the outer shell scattering is dominated by the heavier zinc atoms. The best fit to the experimental EXAFS spectrum and associated Fourier transform of the low temperature spectrum is illustrated in Fig. 3, and Table 1 shows the comparison between the parameters derived from EXAFS and the crystal structure. The EXAFS distances for both oxygen and zinc backscatterers are in excellent agreement with the crystal structure at both temperatures, with the Debye-Waller factors slightly lower at low temperature due to the reduced thermal motion. The first peak in the Fourier transform is due to the coordinated oxygen atoms,

and was modelled using two shells, with 1.6 oxygens at 1.96 Å from the contribution of the tetrahedral zinc atoms and 3.6 oxygens at 2.07 Å from the octahedral zinc atoms. Simulations with just one shell of 5.2 oxygen backscatterers at an average distance gave significantly poorer fits to the experimental spectrum. This demonstrates that EXAFS can be used to give an indication of the coordination environment of a cation distributed over several different sites, and may distinguish between bond lengths which differ by 0.10 Å or more.

(ii) *Aurichalcite*. The coordination environments of the four metal sites in aurichalcite (Harding *et al.* 1994) are shown in Table 2, omitting oxygen and carbon backscatterers beyond the inner coordination sphere. The multiplicities of sites M1:M2:M3:M4 in the crystal structure are 1:2:1:1. In all four sites there is a wide range of metal oxygen distances in the first coordination shell, but only in sites M2 and M4 are there two distinct groups of distances, with the axial oxygens significantly more distant than the equatorial oxygens in both sites. Therefore it would be expected that if either metal preferentially occupied these sites the EXAFS simulation would require a split inner coordination sphere, whereas in sites M1 and M3 a single shell would suffice. In the outer shells, although there are metal backscatterers at similar distances in all the sites, there are differences in the numbers of scatterers in each shell which could reveal which sites each metal occupied.
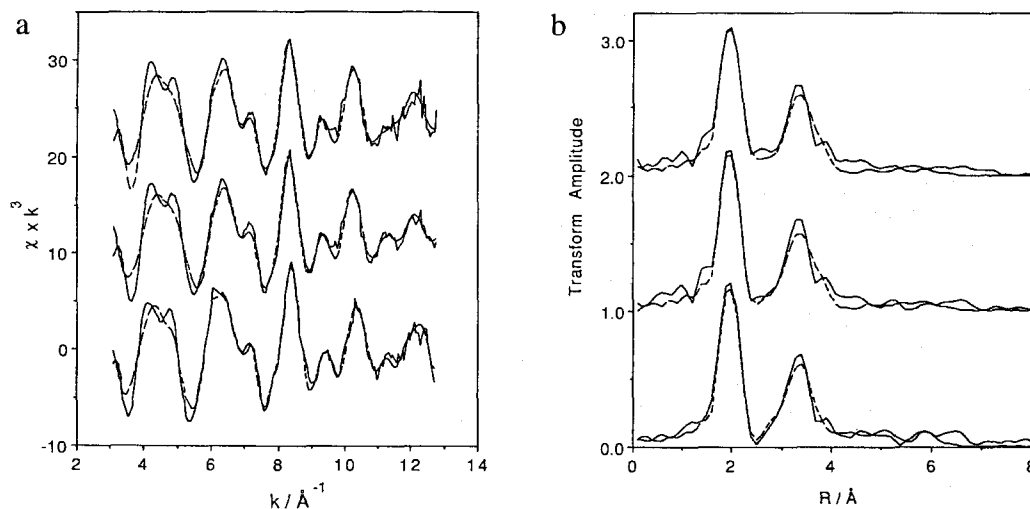
FIG. 4. (*a*) 80K Cu EXAFS (solid lines) and the corresponding best fits (broken lines) of aurichalcite. BM 1964,702 (top), BM 1983,97 (middle) and BM 1937,1355 (bottom). (*b*) Fourier transforms of the 80K Cu EXAFS (solid lines) and the corresponding best fits (broken lines) of aurichalcite. BM 1964,702 (top), BM 1983,97 (middle) and BM 1937,1355 (bottom).

TABLE 2. Radial distribution of atoms around each metal site in aurichalcite (Harding *et al.*, 1994) excluding light atoms beyond the inner coordination sphere

Shell	M1 R/Å	Range/Å	Shell	M2 R/Å	Range/Å	Shell	M3 R/Å	Range/Å	Shell	M4 R/Å	Range/Å
6 × O	2.121	1.937–2.243	4 × O	1.988	1.930–2.013	4 × O	1.965	1.948–1.998	4 × O	2.029	1.980–2.144
—	—	—	2 × O	2.346	2.313–2.379	—	—	—	1 × O	2.352	—
4 × M	3.108	3.050–3.166	5 × M	3.179	3.050–3.261	—	—	—	2 × M	3.261	—
2 × M	3.557	—	2 × M	3.512	3.485–3.539	7 × M	3.548	3.485–3.673	1 × M	3.673	3.883–4.078
2 × M	3.883	—	1 × M	4.078	—	—	—	—	4 × M	3.981	—
—	—	—	—	—	—	—	—	—	2 × M	4.405	—
1 × M	5.040	—	5 × M	5.373	5.293–5.513	2 × M	5.099	—	1 × M	5.040	—
7 × M	5.403	5.294–5.513	5 × M	5.682	5.610–5.829	5 × M	5.311	5.293–5.328	2 × M	5.293	—
1 × M	5.879	—	—	—	—	8 × M	5.775	5.655–5.928	7 × M	5.764	5.610–5.928

TABLE 3. Best fit EXAFS parameters for aurichalcite Cu K-edge spectra at ambient temperature and ca. 80K. The R-factors at ambient and ca. 80K are 28.7 and 25.6 for BM 1964,702, 28.4 and 29.1 for BM 1983,97 and 26.1 and 25.0 for BM 1937,1355

Sample	Shell*	80 K		Ambient	
		R/Å	$2\sigma^2/\text{Å}^2$	R/Å	$2\sigma^2/\text{Å}^2$
BM 1964,702	4.0 × O	1.97	0.008	1.96	0.008
	1.5 × O	2.36	0.008	2.35	0.015
	3.5 × Zn/Cu	3.14	0.020	3.13	0.023
	1.5 × Zn/Cu	3.53	0.007	3.54	0.010
	2.5 × Zn/Cu	3.80	0.029	3.78	0.026
	1.0 × Zn/Cu	4.50	0.021	4.54	0.018
	3.5 × Zn/Cu	5.36	0.031	5.35	0.050
	6.0 × Zn/Cu	5.77	0.038	5.75	0.040
BM 1983,97	4.0 × O	1.97	0.006	1.96	0.008
	1.5 × O	2.35	0.011	2.35	0.015
	3.5 × Zn/Cu	3.14	0.020	3.13	0.023
	1.5 × Zn/Cu	3.53	0.008	3.54	0.010
	2.5 × Zn/Cu	3.81	0.029	3.78	0.026
	1.0 × Zn/Cu	4.49	0.021	4.54	0.018
	3.5 × Zn/Cu	5.33	0.026	5.35	0.050
	6.0 × Zn/Cu	5.84	0.030	5.75	0.040
BM 1937,1355	4.0 × O	1.97	0.006	1.97	0.007
	1.5 × O	2.38	0.011	2.38	0.015
	3.5 × Zn/Cu	3.14	0.018	3.14	0.019
	1.5 × Zn/Cu	3.54	0.006	3.56	0.009
	2.5 × Zn/Cu	3.78	0.022	3.79	0.021
	1.0 × Zn/Cu	4.53	0.016	4.54	0.018
	3.5 × Zn/Cu	5.36	0.031	5.35	0.050
	6.0 × Zn/Cu	5.77	0.023	5.76	0.031

* Average of sites M2 and M4

The spectra of both the edges in all the samples were simulated using various models made up of averages from different combinations of sites, representing different distributions of cations among the four sites. The coordination numbers were fixed for each model, and the absorber-scatterer distances and Debye-Waller factors allowed to float. The best fit parameters for the copper spectra are given in Table 3, and those of the zinc spectra in Table 4. The EXAFS and Fourier transforms of the best fits at low temperatures are illustrated in Figs 4 and 5. Although there are no clear differences between the zinc sites or the copper sites in the three samples, there are differences between the copper and zinc in each sample. In samples BM 1964,702 and BM 1983,97, with copper to zinc ratios of ca. 2:3, the best fits for the copper spectra are with a model which is an average of sites M2 and M4, which both have the inner coordination sphere split into two shells. The zinc spectra do not show this

split, and are best fitted with an average of sites M1 and M3. Though sample stoichiometry and inter-site mass balance considerations show that some of the zinc must occupy sites M2 and M4 the improvement in the fits when the first shell was split did not justify the extra parameters needed for the simulation. In sample BM 1937,1355, in which the ratio of copper to zinc is ca. 1:3, the fits to the copper spectra with a model in which the copper occupied both sites M2 and M4 were slightly better than fits in which the copper occupied solely one site. The zinc spectra of this sample could be fitted reasonably well with an average of sites M1 and M3, but in this case the fits were improved by the addition of an extra shell of oxygens at 2.16 Å, confirming that a significant amount of zinc occupies site M2 or M4, or both. The difference in the two metal-oxygen bond lengths (0.17 Å) is significantly less than in the copper fits (0.38–0.41 Å), explaining why it was not possible to resolve this split in the other two samples, in which a

TABLE 4. Best fit EXAFS parameters for aurichalcite Zn K-edge spectra at ambient temperature and *ca.* 80K. The R-factors at ambient and *ca.* 80K are 25.0 and 23.1 for BM 1964,702, 27.2 and 24.3 for BM 1983,97 and 25.8 and 23.7 for BM 1937,1355

Sample	Shell*	80 K		Ambient	
		R/Å	$2\sigma^2/\text{Å}^2$	R/Å	$2\sigma^2/\text{Å}^2$
BM 1964,702	5.0 × O	1.98	0.015	1.98	0.016
	2.0 × Zn/Cu	3.12	0.022	3.12	0.025
	4.5 × Zn/Cu	3.52	0.014	3.53	0.025
	1.0 × Zn/Cu	3.95	0.044	3.97	0.051
	1.5 × Zn/Cu	5.06	0.027	4.92	0.033
	6.0 × Zn/Cu	5.31	0.020	5.32	0.030
	4.5 × Zn/Cu	5.96	0.023	5.93	0.029
BM 1983,97	5.0 × O	1.98	0.015	1.97	0.016
	2.0 × Zn/Cu	3.10	0.023	3.11	0.024
	4.5 × Zn/Cu	3.52	0.019	3.53	0.025
	1.0 × Zn/Cu	3.96	0.045	3.97	0.051
	1.5 × Zn/Cu	5.06	0.030	4.92	0.033
	6.0 × Zn/Cu	5.32	0.025	5.31	0.030
	4.5 × Zn/Cu	5.93	0.028	5.91	0.029
BM 1937,1355	3.4 × O†	1.99	0.012	1.99	0.014
	0.6 × O†	2.16	0.009	2.16	0.010
	2.0 × Zn/Cu	3.13	0.019	3.14	0.022
	4.5 × Zn/Cu	3.56	0.021	3.57	0.027
	1.0 × Zn/Cu	3.95	0.040	3.97	0.052
	1.5 × Zn/Cu	5.11	0.035	5.11	0.046
	6.0 × Zn/Cu	5.34	0.028	5.34	0.030
	4.5 × Zn/Cu	5.96	0.031	5.98	0.035

* Average of sites M1 and M3
† Adjusted to include contribution from sites M2/M4

lower porportion of the zinc occupies sites *M2* and/or *M4*. The outer shells of metal backscatterers are also consistent with these models. In all of the copper spectra there are contributions from metal back-scatterers between 4 Å and 5 Å, characteristic of sites *M2* and *M4*, which are not present in the zinc spectra. The shell at *ca.* 3.5 Å, present in all the analyses, makes a bigger contribution to the zinc than the copper spectra. In Table 2 it is clear that there are more scatterers at this distance in sites *M1* and *M3* than in *M2* and *M4*.

Summary

From the Cu 2p XAS it is clear that the copper present in aurichalcite is divalent and peak asymmetry suggests that copper might be present in more than one of the four possible metal sites. Although it is not possible from the EXAFS data to extract accurate quantitative information about the metal distribution in the sites, it is clear that in two aurichalcite samples with *ca.* 3:2 Zn:Cu ratio the zinc atoms occupy mainly the *M1* and *M3* sites, with at least 80% of the copper atoms in sites *M2* and *M4*. In the third sample, with a 3:1 Zn:Cu ratio the best fits to the EXAFS spectra are with the copper atoms occupying both *M2* and *M4*, with the zinc atoms in sites *M1* and *M3*, with some contribution from zinc atoms in sites *M2* and *M4*. This is consistent with the known coordination properties of the two metals: copper atoms occupy Jahn-Teller distorted sites in minerals such as azurite, whereas zinc usually occurs in symmetrical octahedral and tetrahedral sites, for example in smithsonite and zincite respectively. These EXAFS data substantially enhance the structural understanding of aurichalcite and provide clear Cu/Zn ordering characteristics across four distinct metal sites. Such information has not been attained by X-ray diffraction due to the similarity of the scattering characteristics of copper and zinc.
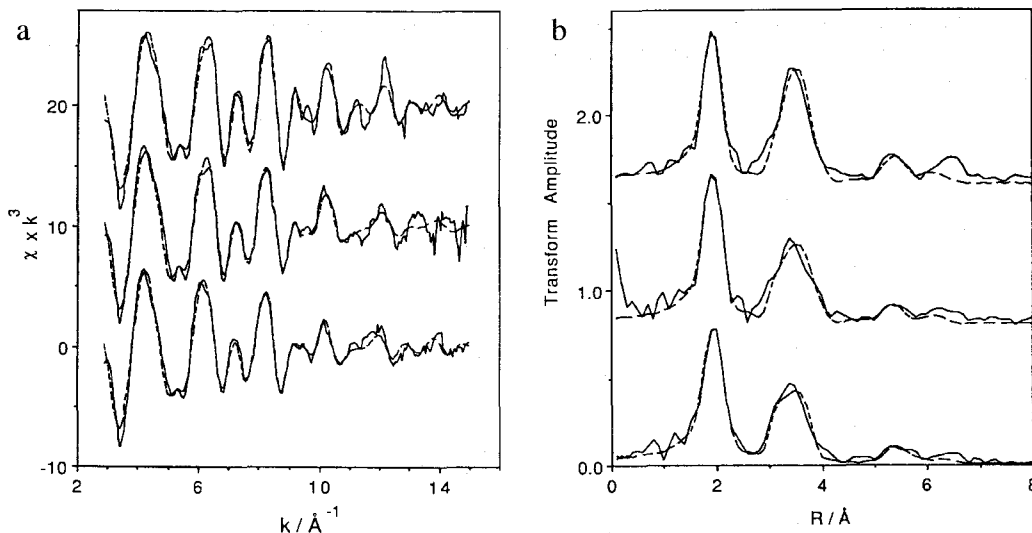
FIG. 5. (a) 80K Zn EXAFS (solid lines) and the corresponding best fits (broken lines) of aurichalcite. BM 1964,702 (top), BM 1983,97 (middle) and BM 1937,1355 (bottom). (b) Fourier transforms of the 80K Zn EXAFS (solid lines) and the corresponding best fits (broken lines) of aurichalcite. BM 1964,702 (top), BM 1983,97 (middle) and BM 1937,1355 (bottom).

References

Binsted, N., Campbell, J.W., Gurman, S.J. and Stephenson, P.C. (1991) CCLRC Daresbury Laboratory EXCURV92 Program.

Braithwaite, R.S.W. and Ryback, G. (1963) Rosasite and aurichalcite and associated minerals from Heights of Abraham, Matlock Bath, Derbyshire, with a note on infrared spectra. *Mineral. Mag.*, **33**, 441–9.

Couves, J.W., Thomas, J.M., Waller, D., Jones, R.H., Dent, A.J., Derbyshire, G.E. and Greaves, G.N. (1991) Tracing the conversion of aurichalcite to a copper catalyst by combined X-ray absorption and diffraction. *Nature*, **354**, 465–8.

Ghose, S. (1964) The crystal structure of hydrozincite, $Zn_5(OH)_6(CO_3)_2$. *Acta Cryst.*, **17**, 1051–7.

Gurman, S.J., Binsted, N. and Ross, I. (1984) A rapid, exact, curved wave theory for EXAFS calculations. *Journal of Physics C: Solid State Physics*, **20**, 4005–12.

Harding, M.M., Kariuki, B.M., Cernik, R. and Cressey, G. (1994) The structure of aurichalcite, $(Cu,Zn)_5(OH)_6(CO_3)_2$, determined from a microcrystal. *Acta Cryst.*, **B 50**, 673–6.

Hedin, L. and Lundqvist, S. (1969) Effects of electron-electron and electron-phonon interactions on the one electron states of solids. *Solid State Physics*, **23**, 1–181.

Herman, R.G., Bogdan, C.E., Kumler, P.L. and Nuszkowski, D.M. (1993) Preparation and character-

ization of hydrocarbonate precursors that yield successful alcohol synthesis catalysts. *Materials Chemistry and Physics*, **35**, 233–9.

Jambor, J.L. and Pouliot, G. (1965) X-ray crystallography of aurichalcite and hydrozincite. *Canad. Mineral.*, **8**, 385–9.

Lee, P.A. and Pendry, J.B. (1975) Theory of the extended X-ray absorption fine structure. *Physical Review*, **B11**, 2795–811.

MacDowell, A.A., West, J.B., Greaves, G.N. and van der Laan, G. (1988) Monochromator and beamline for soft X-ray studies in the photon range 500 eV–5keV. *Review of Scientific Instruments*, **59**, 843–52.

Pollard, A.M., Spencer, M.S., Thomas, R.G., Williams, P.A., Holt, J. and Jennings, J.R. (1992) Georgeite and azurite as precursors in the preparation of coprecipitated copper-zinc oxide catalysts. *Applied Catalysis*, **A 85**, 1–11.

Porta, P., De Rossi, S., Ferraris, G. and Pompa, F. (1991) Characterization of copper-zinc mixed oxide system in relation to different precursor structure and morphology. *Solid State Ionics*, **45**, 35–41.

Schofield, P.F., Henderson, C.M.B., Redfern, S.A.T. and van der Laan, G. (1993) Cu 2p absorption spectroscopy as a probe for site occupancy of $(Zn_xCu_{1-x})WO_4$ solid solution. *Phys. and Chem. of Minerals*, **20**, 375–81.

Sengupta, G., Sharma, R.K., Sharma, V.B., Mishra, K.K., Kundu, M.L., Sanyal, R.M. and Dutta, S.

(1995) Effect of incorporation of Al^{3+} ion on the structure of Cu-Zn coprecipitate. *Journal of Solid State Chemistry*, **115**, 204−7.

van der Laan, G., Pattrick, R.A.D., Henderson, C.M.B. and Vaughan, D.J. (1992) Oxidation state variations in copper minerals studied with Cu 2p X-ray absorption spectroscopy. *Journal of Physics and Chemistry of Solids*, **53**, 1185−90.